Multi-Objective Optimization Design of Lever Arm based on Kriging Model

Yirui Zhang, Shengli Zhao, Zongqi Man, Baojun Qu, Xiangyu Tian, Qijun Zhu, Kai Zhang

Abstract—**An optimal design method based on the combination of Kriging model and MOGA was proposed to solve the lightweight problem of the lever arm of the lever loaded air spring experimental equipment. Using the lever arm as a research object, the maximum stress condition was determined by combining the working principle with multi-angle and multi-working condition static simulation, and the lever arm's design variables were parameterized. Second, the initial sample design points were obtained using the OSF sampling method, the Kriging response surface model was developed, 60 groups of verification points were reselected, and the accuracy of response surface prediction was tested using the complex correlation coefficient and root mean square error. Third, the mathematical model of MOGA optimization was developed based on the response surface model's high fit degree, with the objective function of minimizing the lever arm mass and the constraints of maximum equivalent stress and deformation. The optimal design parameters of the lever arm were obtained after 9 iterations and 9852 evaluations. The optimized lever arm mass was reduced by 12.8%, the maximum equivalent stress and maximum deformation were reduced, and the expected design effect was achieved after the installation of experimental equipment and engineering verification, which proves the feasibility and reliability of the proposed optimization method. It was worth mentioning that this optimization design method was considered to provide a certain reference for the optimization design of similar parts.**

Index Terms—**Lever Arm, Kriging Model, Response Surface Method, Multi-Objective Optimization**

Manuscript received June 29, 2024; revised December 5, 2024.

This work was supported in part by the Natural Science Foundation of China under Grant 12202252, the Natural Science Foundation of Shandong Province under Grant ZR2022QE018, and the Key Technology R&D and Industrialization Project of Automotive Intelligent Suspension System of Shandong Province under Grant 2023CXGC010211.

Yirui Zhang is a lecturer at the School of Traffic and Vehicle Engineering at Shandong University of Technology, Zibo 255000, China.(corresponding author, e-mail: zyr86913@163.com).

Shengli Zhao is a postgraduate student at the School of Traffic and Vehicle Engineering at Shandong University of Technology. Zibo 255000, China. (e-mail: 15689045693@163.com).

Zongqi Man is a postgraduate student at the School of Traffic and Transportation at Beijing Jiaotong University. Beijing 100044, China. (e-mail: mzq991101@163.com).

Baojun Qu is a lecturer at the School of Traffic and Vehicle Engineering at Shandong University of Technology, Zibo 255000, China. (e-mail: qbj22@sina.com).

Xiangyu Tian is a lecturer at the School of Traffic and Vehicle Engineering at Shandong University of Technology, Zibo 255000, China. (e-mail: tianxy@sdut.edu.cn).

Qijun Zhu is a postgraduate student at the School of Traffic and Vehicle Engineering at Shandong University of Technology, Zibo 255000, China. (e-mail: zqj614103@163.com).

Kai Zhang is a deputy senior engineer of Shandong Jinding Zhida Group Co., LTD, Zibo 255000, China. (e-mail: 841213463@qq.com).

I. Introduction

The lever arm we designed was basically applied in the air spring experimental equipment to enlarge the proportion of the load on the hook end of the lever to the air spring, and thus, achieving the purpose of simulating large mass loading at the upper end of the air spring. Considering the welding of the lever arm and the selection of materials, the unreasonable size design has a direct impact on the reliability of the experimental equipment, and even affects the safety of the experiment [1]. To ensure the reliability of the experimental equipment, most of the available simple parts were designed to be exceptionally heavy, or the design dimensions of the parts were repeatedly modified according to finite element simulation and work experience [2, 3]. As a result, the design process of parts was tedious, and the design of multi-size of parts was unreasonable, resulting in a waste of material performance. Accordingly, diverse optimization methods were proposed for structural optimization design in multi-field applications[4].

Kouritem A et al. analyzed the material structure of the robot linkage structure by finite element simulation in ansys, and optimized the robot arm using the genetic algorithm, which improved the safety factor of the structure and avoided working under conditions close to natural frequencies [5]. Maradey Lázaro J G et al. analyzed and predicted the load on the vehicle chassis in the real world and optimized its geometry relying on finite element software [6]. Pappalardo C M et al. redesigned the aircraft door lock bolt through finite element analysis and topology optimization, and established a stress analysis system for boundary conditions, which significantly improved the system performance of the aircraft door by comparing the original mechanical subsystem [7]. Shui L et al. established an empirical model for minimizing the mass, minimizing deformation, and maximizing the natural frequency of the battery pack shell through the experimental methods of central composite design (CCD) and artificial neural network (ANN), and optimized the model using the non-dominant sequencing genetic algorithm (NSGA II), which mitigated the mass of the battery module of the electric vehicle and reduced the vibration impact of the battery pack [8]. Martinez W et al. introduced a multi-objective optimization algorithm to obtain a Pareto frontier by evaluating the effects of different materials and sizes on the structure by evaluating the results of the modeling phase [9]. Chandrasekhar A et al. accelerated the topology optimization of variable density structures by driving the training of obtained data with the help of machine learning techniques [10]. Kurtuluş et al. combined the Harris hawks optimization algorithm with the simulated annealing

algorithm to improve the global convergence speed and optimize the structural design of the guardrail [11]. The response surface method is a more common method and is mainly adopted to reduce the computational effort of engineering analysis. Zhao W et al. ensured the accuracy of fitting the response surface by substituting control points for design points during sampling, and verified the structural reliability of the proposed method by combining five examples [12]. Yang et al. performed a numerical analysis of the spiral separator and obtained the correlation between structural variables and performance indicators by response surface method [13]. Park C et al. determined the optimal lead curve and robust tooth surface design by response surface method and multi-objective optimization to solve the gear noise problem [14], and screened out the influence of experimental transmission error on candidate design variables by ANOVA.

In the study of the lightweight design of the lever arm, the maximum force condition of the lever arm was determined, and the parametric modeling and static analysis of the lever arm size were carried out. Then, the design parameter variables were clarified and 25 groups of design sample points were generated based on the Best Filling Design (OSF) method, the response surface model was constructed by Kriging algorithm and the accuracy of the response surface was verified, and the target variables were optimized and solved by multi-objective genetic algorithm. Finally, the optimal solution of the design variables was remodeled, and the finite element verification comparison and multi-angle test were carried out. In summary, the optimized design method satisfies the design requirements, effectively reduces the mass of the lever arm, and saves the material cost to a certain extent.

II. Lever Arm Modeling and Static Characteristics Analysis

A. Working Principle

According to the project requirements and the pre-test function, the load was amplified and applied to the air spring by following the principle of the Chinese lever scale and using the lever structure, which contributes to meeting the requirements of load application during the air spring performance test. The mechanical part of the test device was shown in Fig. 1, including the lever pressure part, the load test part and the bottom load-bearing part. The specific working principle was as follows. The lever application part was mainly composed of a weight, a lever arm assembly, a supporting column and a load roller. The weight was connected to one end of the lever arm assembly through a hook, and the other end was hinged in the connecting through holes of different heights of the supporting post. The load roller was fixed under the lever arm, and the vertical force above the upper roof was always maintained by the load roller. The upper roof of the load uses the vertical sliding shaft as the horizontal limit and support to release the vertical degree of freedom at the same time, and provides the necessary compressed air for the air spring through the high pressure air source, so as to achieve the function that the air spring can stretch freely longitudinally under the load. The bottom load-bearing part was mainly responsible for the fixed installation of the air spring and the sliding shaft limiting device, and was fixedly connected to the cast iron platform through the supporting foot to ensure the structural stability of the device during the test. The flange force sensor was installed at the lower end of the upper roof and a linear displacement sensor was installed between the upper and lower roof to detect the weight of the load and the height change of the air spring in real time. In the above-mentioned mechanical structure, the force and deformation of the lever arm were particularly important to the reliability of the test device and the smooth progress of the test, so this work focuses on the analysis and verification of the design and strength check part of the lever arm.

B. Force Analysis of Lever Arm

The lever arm was used as the research object, as shown in Fig. 2. During the inflation and deflation of the air spring, the upper upper roof slides longitudinally under the constraints of the sliding shaft, and the weight borne by the load cell mainly comes from the weight loaded by the lever arm and the weight of the upper upper roof and the load pulley.

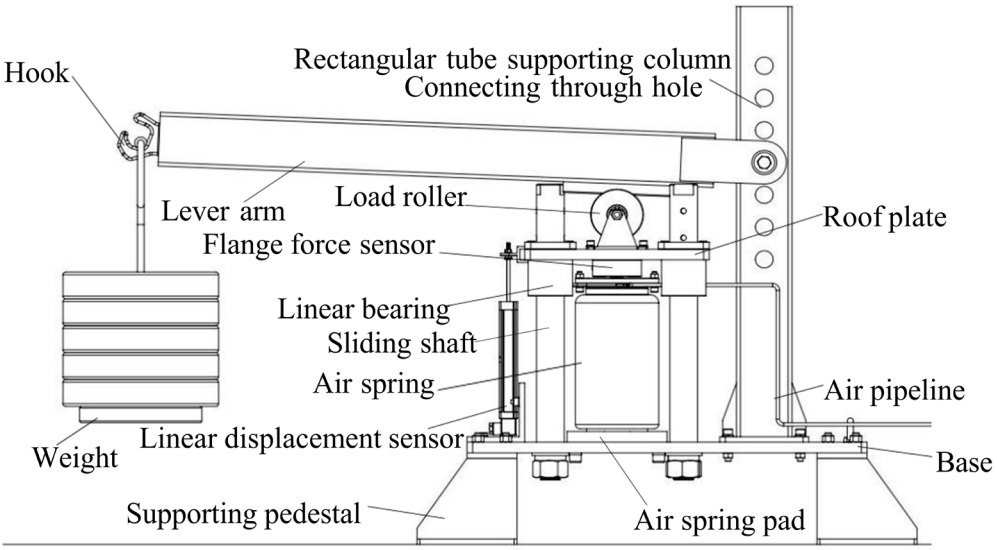

Fig. 1. Schematic diagram of the structure of the lever loading device

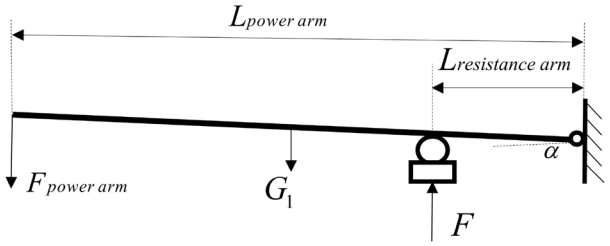

Fig. 2. Schematic diagram of force analysis of lever arm assembly

$$F = F_{r1} + F_{r2} \tag{1}$$

Where, F represents the weight shown by the load cell, F_{r1} represents the weight of the load pulley when the lever arm was pressed down when the weight was loaded, F_{r2} represents the weight of the load pulley when the self-weight of the lever arm was pressed down.

When the air spring reaches steady-state equilibrium, it was based on the lever equilibrium formula:

$$L_r F_r = L_p F_p \tag{2}$$

Where, F_p represents the weight of the loaded weight; L_p represents the horizontal distance from the hook to the hinged shaft; L_r represents the horizontal distance from the center point of the load pulley to the hinged shaft;

In the design of the lever arm, the ratio of the resistance arm to the power arm when the lever arm is horizontal is:

$$L_r / L_p = 1/4 \tag{3}$$

When the air spring was inflated and deflated, the resistance arm L_r does not change, that is:

$$L\cos\alpha F_p = \frac{L}{4} F_{r1} \tag{4}$$

$$\frac{L}{2}\cos\alpha G_1 = \frac{L}{4} F_{r2} \tag{5}$$

Where, G_1 represents the weight of the lever arm assembly, L represents the length of the lever arm.

The height of the air spring was z when the lever arm was horizontal, and the height of the air spring was z_a when the inflation and deflation were completed to reach equilibrium:

$$\tan\alpha = \frac{|z_a - z|}{L_r} = \frac{4|z_a - z|}{L} \tag{6}$$

That is, the angle α between the lever arm and the horizontal:

$$\alpha = \arctan\left(\frac{4|z_a - z|}{L}\right) \tag{7}$$

Eqs. (1) and (7) were combined to give the load cell a weight that:

$$F = 2\cos\left[\arctan\left(\frac{4|z_a - z|}{L}\right)\right](2F_p + G_1) \tag{8}$$

Eq. (8) shows that when the lever arm reaches dynamic equilibrium at multiple angles, the air spring bears the maximum load in the horizontal position.

C. Establishment of Finite Element Model

The original three-dimensional model of the lever arm was established using SolidWorks. In order to ensure the improvement of the mesh mass and the accuracy of the finite element simulation results, the lever arm was properly simplified according to the Saint-venant principle on the premise that the basic structural characteristics of the lever arm remain unchanged, ignoring some features such as fillet, chamfer and so on [15, 16]. The material of the lever arm was Q235 carbon structural steel, and its mechanical properties were shown in Table 1, and the grid is shown in Fig. 3. When constructing the finite element model through ansys, the meshing method of tetrahedral element was adopted, the size of the element was set to 5mm, the center of the span angle was set to fine, and the final model contains 121233 elements and 207712 nodes, and the mesh mass was 0.83945, which satisfies the mesh standard of finite element analysis.

Fig. 3. Finite element model of lever arm

TABLE I
MECHANICAL PROPERTY PARAMETERS OF Q235 STEEL

Materials	Density $\rho/(kg\cdot m^{-3})$	Elastic modulus /MPa	Poisson's ratio	Yield strength/MPa
Q235	7850	200	0.3	235

D. Static Analysis

In view of the fact that one end of the lever arm was hinged to the supporting column by the connecting shaft and does not produce relative displacement, a fixed constraint was imposed on it; the welding slider at the lower end of the lever arm was in contact with the load pulley, and the lever arm bears the supporting force upward of the load pulley during dynamic balance, so the middle position of the welding slider at the lower end of the lever arm was locally fixed. According to the actual working conditions and the test requirements of the air spring, the maximum load of a single air spring was about 800kg, so the vertical load at the hook was 2000N, and the constraint of the lever arm was shown in Fig. 4.

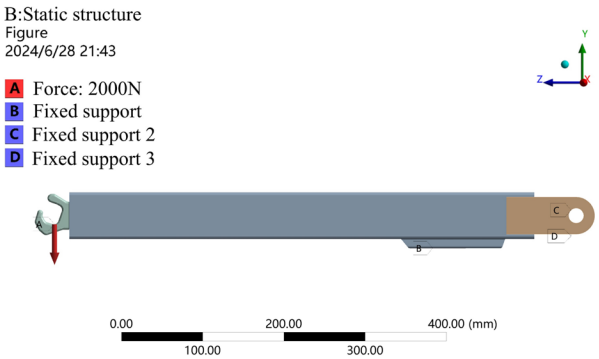

Fig. 4. Lever arm load and constraint

Through the finite element analysis of the static characteristics of the lever arm, the stress cloud map, deformation cloud map and safety factor cloud map [17, 18] were obtained, as shown in Fig. 5. The analysis of the loaded lever arm suggested that the maximum deformation of the lever arm appears at the end of the hook and the size was 0.75597mm. The maximum equivalent stress appeared at the leftmost end of the connection between the lower end of the lever arm and the welding slider, the size was 123.82MPa,

which was due to the phenomenon of stress concentration caused by the simplification of the model. According to the yield strength 235MPa of Q235 ordinary carbon steel, the maximum equivalent stress of the lever arm was far less than the yield strength of the material, which meets the design requirements. In addition, the equivalent stress and deformation in most areas of the lever arm and the lifting lug were extremely small, so it was considered that the lever arm structure has a certain optimization space.

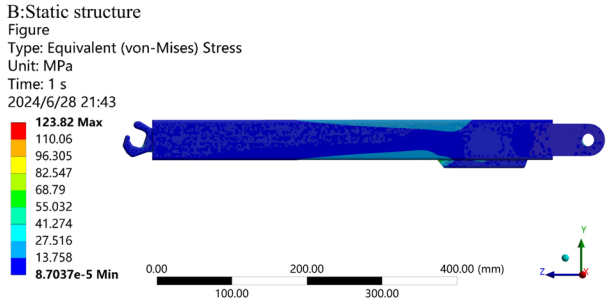

a) Stress cloud diagram of lever arm

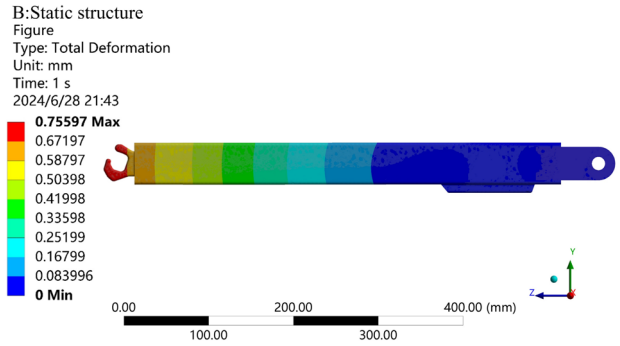

b) Deformation cloud picture of lever arm

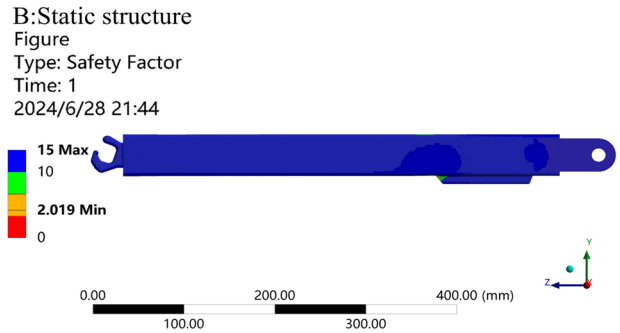

c) Contour of the safety factor of the lever arm

Fig.5. Contour of the static analysis of the lever arm

E. Verification of Static Properties from Multiple Angles

When the lever arm reaches dynamic balance in multi-angle position, the relationship between the supporting force of the welding slider at the lower end of the lever arm and the maximum equivalent stress and maximum deformation of the lever arm structure can be understood through the analysis of static characteristics. According to table 2 and Fig. 6, the maximum stress of the lever arm was 123.82MPa, the maximum deformation was 0.75597mm, and the minimum safety factor was 2.019 when the angle between the lever arm and the horizontal changes from 25 ° to -15 °. The analysis implies that when the lever arm was in the horizontal position and receives the maximum support force of the load pulley, the equivalent stress and deformation of the lever arm were the largest, indicating that the strength and safety performance of the lever arm only need to be considered in the horizontal state in the subsequent optimization process.

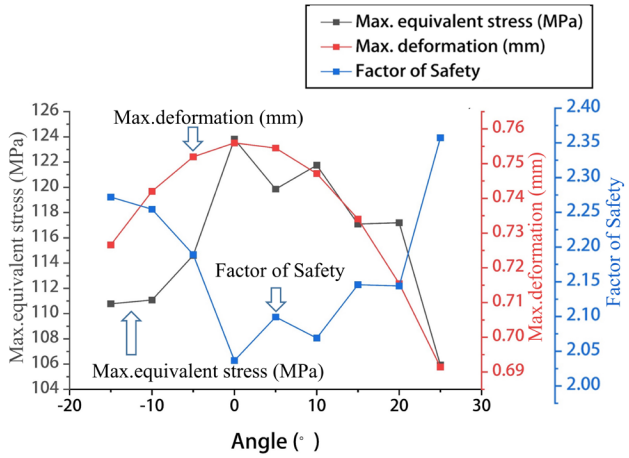

Fig.6. Polyline diagram of multi-angle static characteristics

III. Optimization of the Response Surface of the Lever Arm

A. Optimize the Process based on the Response Surface

The common optimization methods of Ansys workbench include topology optimization, size optimization, shape optimization and response surface optimization, among which response surface optimization was extensively applied in the engineering field because it can more intuitively show the relationship between parametric design variables and output variables. In order to reduce the weight of the lever arm and improve the maximum equivalent stress of the lever arm, the optimal design was carried out on the basis of the analysis of static characteristics.

Firstly, a parameterized input model was established for the thickness of the lifting lug, the height of the lug, the inner fillet radius of the lever arm, the thickness of the lever arm and the height of the lever arm. The maximum equivalent stress, maximum deformation, minimum safety factor and lever arm mass were taken as the output parameters of the model.

TABLE II
STRESS, DEFORMATION AND SAFETY FACTOR AT DIFFERENT ANGLES

Lever arm angle /°	25	20	15	10	5	0	-5	-10	-15
Max. stress /MPa	105.93	117.2	117.09	121.75	119.86	123.82	114.61	111.08	110.78
Max. deformation /mm	0.69146	0.71548	0.73408	0.74713	0.75448	0.75597	0.75196	0.74204	0.72658
Min. safety factor	2.36	2.1331	2.1352	2.0534	2.0858	2.019	2.1813	2.2506	2.2692

Secondly, the design sample points were generated by determining the design objectives, the output values of the sample points were calculated, and the response surface model was fitted by the optimization points. The objective function's sensitivity to the design variables was then assessed, as was the response surface's accuracy. Finally, an optimization method was introduced to select the parameter optimization design, and candidate points were chosen to achieve the goal of parameter optimization design. Fig.7 depicts the specific process of optimizing the response surface.

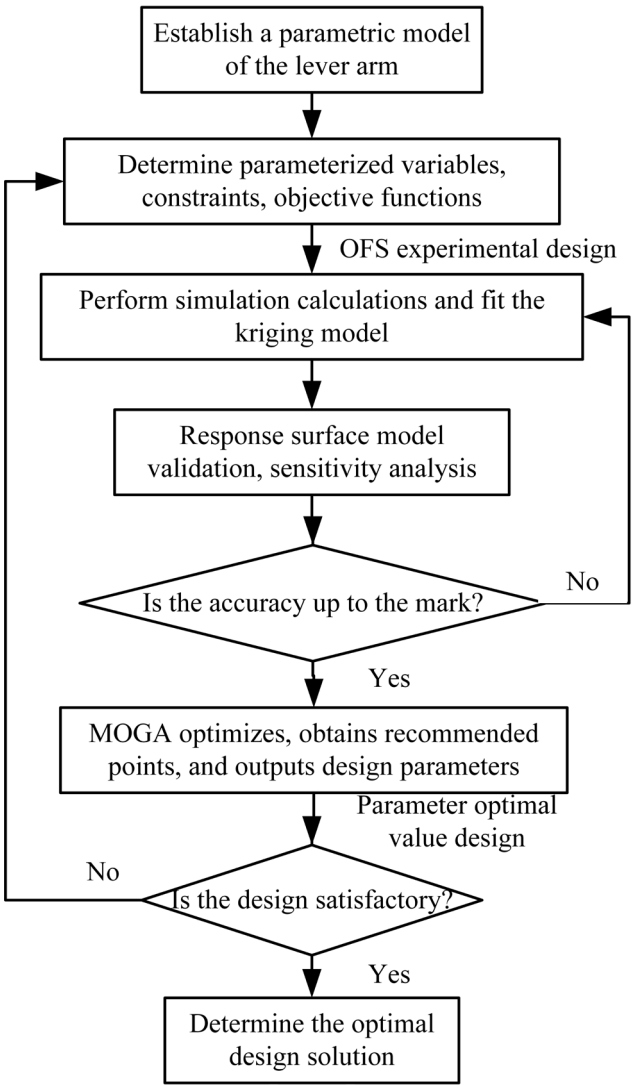

Fig. 7. Flowchart of lever arm optimization based on response surface method

B. Selection of Design Variable

According to the analysis of static characteristics, the stress and deformation in most areas of the lever arm and the position of the lifting lug were small, and its structure has a large safety margin, implying the necessity of re-optimizing the design of the parameter size of the lever arm. Therefore, the fillet should be increased at the connection position between the lower end of the lever arm and the welding slider to avoid excessive stress concentration. It was known that the thickness of lever arm and lug was 10mm. In the process of optimization, the thickness of up and down and left and right of lever arm and the thickness of lugs on both sides should meet the synchronous change of size. In addition, other design variables for optimizing the size of the lever arm were the height of the lever arm, the radius of the inner fillet and the height of the lug. The design variable parameters of the lever arm were shown in Fig. 8. The original size and design standards of the lever arm avoid the mutual interference of the size parameters of the lever arm, and determine the variation range of the size parameters of the lever arm, as shown in Table 3.

TABLE III
VARIATION RANGE OF DESIGN PARAMETERS OF LOAD CROSS ARMS

Design parameters	Name	Initial value /mm	Range of variation /mm
P1	Thickness of lifting lugs	10	5-15
P2	Height of the lifting lugs	80	P5-20
P3	Lever arm inner fillet	1	0.5-5
P4	Lever arm thickness	10	5-15
P5	Lever arm height	100	90-120

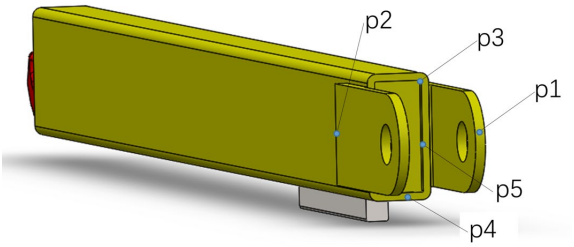

Fig.8. Lever arm design variables

C. Design of Experiment(DOE)

In the design of experiment (DOE), the calculation and accuracy of establishing the response surface model were linked to the experimental design method. In general, the experimental design was to linearly average the known samples in the feasible range of the design variables in order to obtain the optimal sample solution with the least amount of computation. This method basically features the least number of design points to fill the design space [19]. In this work, the optimal space filling design (OFS) was selected as the experimental type design method, which was suitable for more complex response surface algorithms, such as Kriging, Non-Parametric Regression and Neural Networks. However, the OSF design method may not be able to take samples near the endpoints when the sample data was small, which will affect the mass of the response surface in these areas. During the experimental design process, the number of samples was set to 25, the maximum-minimum distance was selected as the design type, and the maximum number of cycles was set to 10 to ensure that the design parameter space was evenly distributed in the process of random sampling of the design space, and the minimum distance between the two design points was maximized, so as to achieve the minimum number to obtain the optimal sampling of the design points. The design points and calculation results were shown in Table 4.

TABLE IV
DESIGN POINTS AND RESULTS OF EXPERIMENTAL DESIGN

No.	P1mm	P3mm	P4mm	P5mm	P2/mm	Max. Stress /MPa	Max. Deformation /mm	Min. safety factor	Mass /kg
1	7.2	2.2	5.2	101.4	81.4	175.83	1.2030	1.42	13.62
2	13.2	3.5	5.6	102.6	82.6	152.83	1.0806	1.64	15.95
3	6.4	3.1	11.2	91.8	71.8	106.22	0.8381	2.35	22.67
4	8.8	4.7	13.6	103.8	83.8	81.91	0.5526	3.05	29.53
5	8.0	3.7	6.0	114.6	94.6	119.71	0.7936	2.09	17.06
6	13.6	3.3	7.6	117.0	97.0	89.04	0.6180	2.81	22.35
7	10.0	4.2	12.0	118.2	98.2	72.54	0.4330	3.45	30.42
8	14.8	2.0	9.2	96.6	76.6	92.74	0.8427	2.70	21.98
9	5.6	1.5	8.8	109.8	89.8	84.80	0.6499	2.95	21.47
10	11.2	2.4	14.8	112.2	92.2	71.53	0.4376	3.50	34.05
11	12.0	0.9	6.4	105.0	85.0	124.91	0.9236	2.00	17.54
12	5.2	4.0	10.0	107.4	87.4	75.60	0.6189	3.31	23.32
13	7.6	4.6	6.8	97.8	77.8	127.68	1.0232	1.96	16.51
14	12.8	1.1	13.2	99.0	79.0	121.89	0.6333	2.05	28.49
15	11.6	4.9	8.4	108.6	88.6	84.80	0.6759	2.95	22.12
16	6.8	1.7	14.0	100.2	80.2	84.03	0.5987	2.98	28.69
17	9.6	1.9	8.0	119.4	99.4	85.35	0.5709	2.93	22.43
18	10.4	2.6	7.2	90.6	70.6	132.64	1.1781	1.88	16.69
19	8.4	0.8	9.6	95.4	75.4	91.37	0.8477	2.74	21.12
20	10.8	2.9	14.4	94.2	74.2	98.27	0.6845	2.54	28.62
21	14.0	1.3	10.8	113.4	93.4	64.07	0.5147	3.90	28.09
22	12.4	4.4	10.4	93.0	73.0	93.18	0.8449	2.68	22.87
23	14.4	3.8	12.4	106.2	86.2	72.86	0.5489	3.43	29.44
24	6.0	2.7	12.8	115.8	95.8	64.40	0.4420	3.88	30.19
25	9.2	0.6	11.6	111.0	91.0	64.91	0.5187	3.85	27.79

D. Mathematical Model Construction of Response Surface Method

Finite element method response surface structure optimization necessitates a large number of sample point sampling to determine the response surface model after many iterations, resulting in a high calculation cost of the model output parameters and complicating the design of multi-parameter structures. Kriging model was capable of analyzing the relationship between design variables and realize fast estimation of eigenvalues of multi-parameter sample response [20, 21] through less sample point sampling operation. The Kriging model has high fitting accuracy when solving the nonlinear model, which can analyze the functional relationship between the response value of the design point and the output variables, but also analyze the error between the response value and the real value according to the verification point, which provides a strong support for the precision fitting degree of response surface and the reliability analysis of lever arm structure design. The Kriging model consists of a polynomial regression function and a stochastic process. The structural response functions include:

$$y(x) = f^T(x)\beta + z(x) \tag{9}$$

Where, $f^T(x)\beta$ represents the regression function of the system polynomial, $f^T(x) = \left[f_1(x), f_2(x), ...f_n(x)\right]^T$, β represents the polynomial regression coefficient matrix, which was expressed as $\beta = [\beta_1, \beta_2, ..., \beta_n]^T$, $z(x)$ represents the random function, which obeys the normal distribution $N(0, \sigma^2)$, and the covariance formula is:

$$Cov[z(x_i), z(x_j)] = \sigma^2 R[r(x_i, x_j)] \tag{10}$$

Where, σ^2 represents the variance of $z(x)$; R represents the covariance matrix of the sample points, which was positively definite along the diagonal. The expression is:

$$R = \begin{bmatrix} r(x_1, x_1) \cdots r(x_1, x_n) \\ \vdots \qquad\qquad \ddots \quad \vdots \\ r(x_n, x_1) \cdots r(x_n, x_n) \end{bmatrix} \tag{11}$$

Where, $r(x_i, x_j)$ represents Spatial functions of x_i and x_j in any N sample points. In order to better fit the accuracy of the response surface model, the most extensively applied was the Gaussian correlation function, which has the following expression:

$$r(x_i, x_j) = \exp(-\sum_{k=1}^{n} \theta_k \mid x_i^k - x_j^k \mid^2) \tag{12}$$

Where, x_i^k, x_j^k components of the design variables; n represents the number of design variables; θ_k represents the uncertain parameter used to fit the model, n was the number of design variables, and k was the component of the sample points x_i^k and x_j^k. θ was calculated as:

$$\theta = \arg\max(-\frac{m}{2}\ln\sigma^2 - \frac{1}{2}\ln \mid R \mid) \tag{13}$$

The estimated values of $\hat{\beta}$ and $\hat{\sigma}^2$ in the response surface feature model were as follows:

$$\hat{\beta} = (F^T R^{-1} F)^{-1} F^T R^{-1} Y \tag{14}$$

$$\hat{\sigma}^2 = \frac{(Y - F\beta)^T R^{-1} (Y - F\beta)}{n} \tag{15}$$

Where, Y represents the response value of the sample point x_i .

After the Kriging response surface model was constructed, the response value $\hat{y}(x_0)$ corresponding to the point x_0 to be measured in the design variable space was expressed as:

$$\hat{y}(x_0) = f^T(x_0)\hat{\beta} + r^T(x_0)\gamma^* \tag{16}$$

Where, $\gamma^* = R^{-1}(Y - F\hat{\beta})$, $r^T(x_0)$ represents the row vector of the correlation function between any sample point and the point to be measured, which was expressed as:

$$r^T(x_0) = \left[R(x_0, x_1), R(x_0, x_0), \cdots, R(x_0, x_n)\right] \tag{17}$$

Therefore, the variance of the estimated feature of the point to be measured is:

$$s^2(x_0) = \hat{\sigma}^2(1 - r^T(x_0)R^{-1}r(x_0)) + \frac{\hat{\sigma}^2(1 - r^T(x_0)R^{-1}r(x_0))^*}{F^T R^{-1} F} \tag{18}$$

E. Response Surface Model Validation and Analysis

In order to verify the accuracy of the fitting of the Kriging response surface model, 60 sets of verification points were generated to test the fitting degree of the response surface model with the maximum equivalent stress, maximum deformation, safety factor and mass of the constructed lever arm to judge the accuracy of the response surface model. In this work, the complex correlation coefficient (R^2) test as well as the root mean square error ($RMSE$) were used to evaluate the accuracy of the response surface. It was calculated as follows:

$$R^2 = 1 - \frac{\sum_{j=1}^{N}[y_{RS}(j) - y(j)]^2}{\sum_{i=1}^{N}[y(j) - \bar{y}]^2} \tag{19}$$

$$RMSE = \frac{1}{N\bar{y}}\sqrt{\sum\left(y - y_{RS}\right)^2} \tag{20}$$

Where, y_{RS} represents the predicted value of the response surface model， y represents the true value of the finite element calculated by the verification point，$\bar{y}$ represents the finite element average for verification point calculations， N represents the number of samples at the validation point.

After calculating the verification point, the equivalent maximum stress, maximum deformation, safety factor and mass of the kriging response surface model predicted value and real value were fitted respectively. As shown in Fig. 9, the complex correlation coefficients (R^2) and root mean square errors ($RMSE$) of the response surface models were all more than 0.95, indicating that the response surface model has high fitting accuracy and meets the needs of design, and can be adopted to optimize the design.

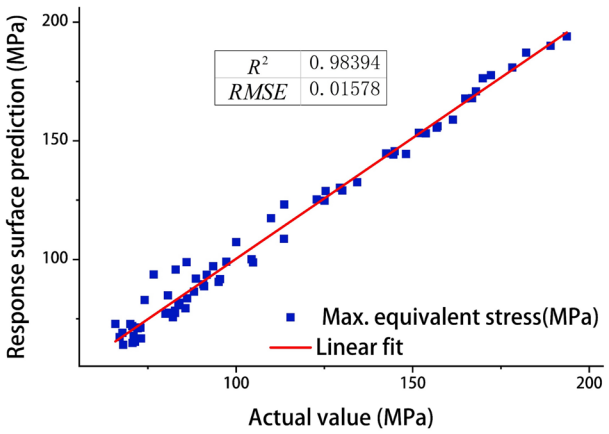

(a) Equivalent stress

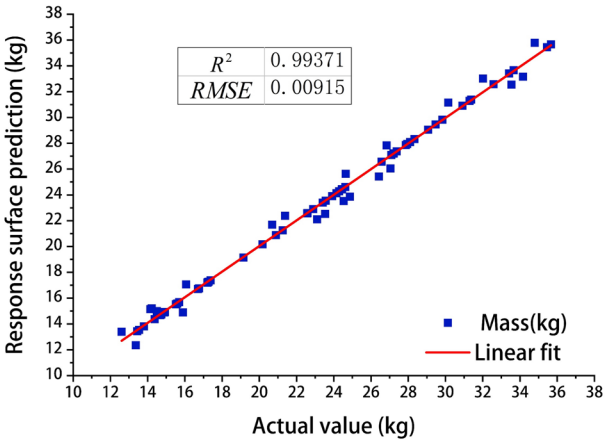

(b) Mass

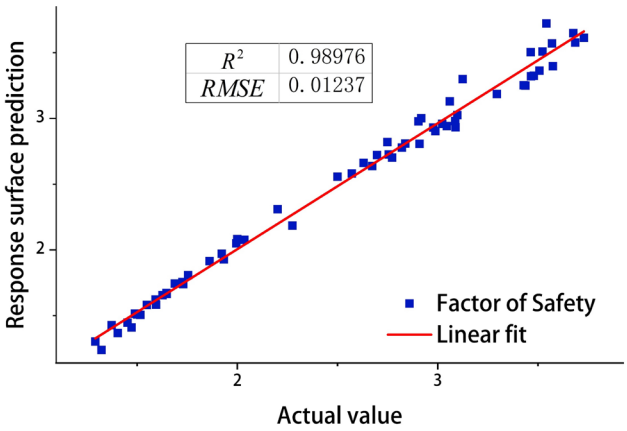

(c) Factor of safety

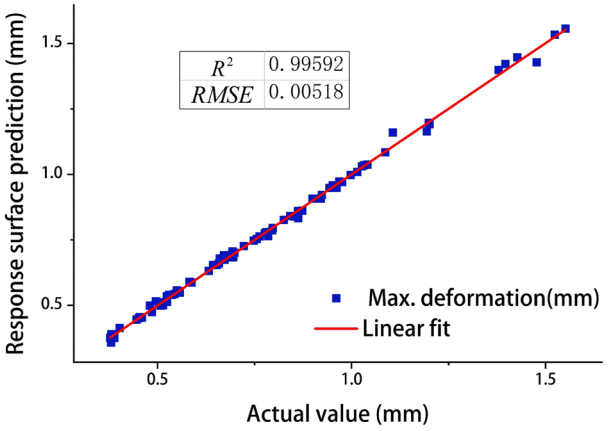

(d) Maximum deformation

Fig. 9. Response surface fitting accuracy

Sensitivity and response surface analysis were important links in the optimization design of response surface. The response surface analysis enables to obtain the influence of various design parameters on the maximum equivalent stress, maximum deformation, minimum safety factor and the mass of the lever arm, so as to determine the optimal range of design variables. The local sensitivity and response surface curves were shown in Figs. 10 and 11, respectively. The results of response surface model reflect the accuracy of local sensitivity analysis. Considering that the height of the lifting lug should be less than the height of the lever arm, P2 was set to be less than 20 mm of P4 in the process of designing variables, and the influence of the height of the lifting lug on the design target variable was not considered in the local sensitivity. Figs. 10 and 11 suggest that the positive and negative values of the column chart in Fig. 10 show the positive and negative correlation between the design variables and the target parameters, in which the parameters p1, p3, p4 and p5 were negatively correlated with stress and deformation, and positively correlated with mass. Among the design variables, p1 and p3 have less influence on the target variable, while p4 and p5 have a higher contribution to the target variable, which corresponds to the maximum stress point located at the lower end of the lever arm and the load slider. Therefore, the thickness and height of the lever arm, as well as the proper optimization of the lug thickness and the radius of the inner fillet of the lever arm, should be optimized on the basis of following the mechanical strength check.

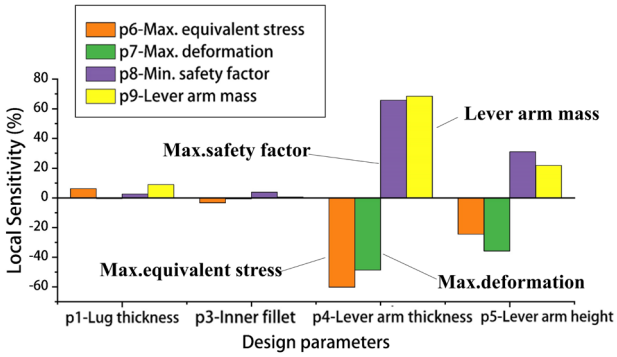

Fig. 10. Local sensitivity

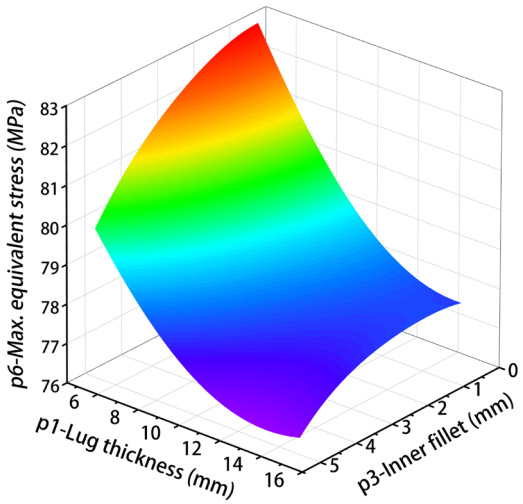

(a) Maximum stress

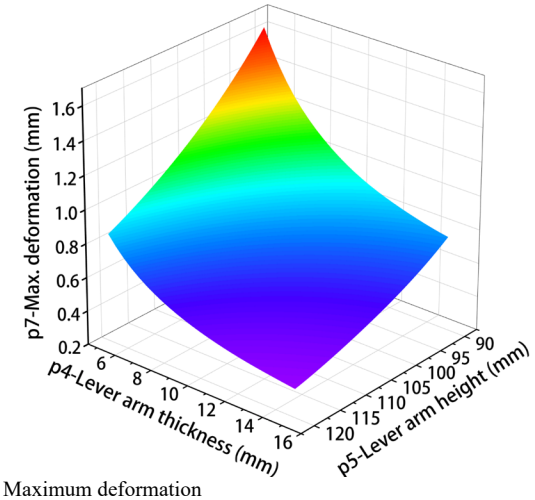

(b) Maximum deformation

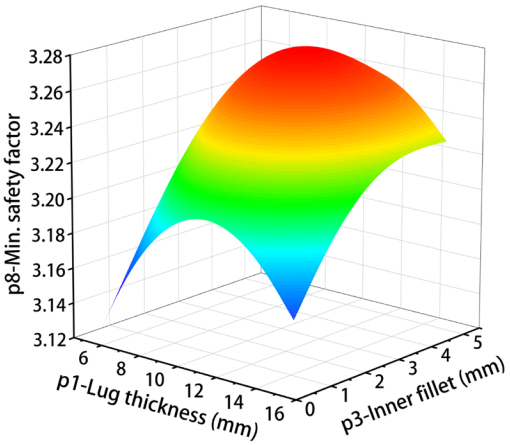

(c) Factor of safety

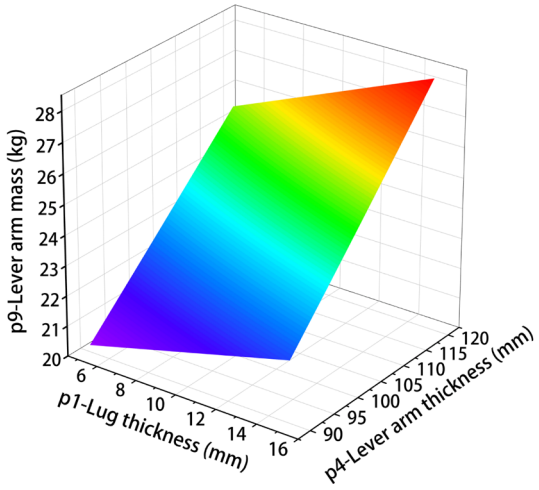

(d) Lever arm mass

Fig. 11. Response surface of lever arm

IV. Optimal Design of Lever Arm

A. Establishment of mathematical model for optimal design

In this study, the purpose of this study was to improve the equivalent stress of the lever arm and reduce the quality of the lever arm redundancy by means of response surface optimization, and to provide three optimization algorithms of screening method (Scrininen), multi-objective optimization (MOGA), and hybrid optimization (AMO) with the help of ansys software. Among them, the multi-objective

optimization algorithm was a multi-objective genetic algorithm based on Pareto sorting, which has a short calculation time, strong global search ability, supports multiple targets and constraints, and was suitable for calculating the maximum and minimum values of multiple parameters, so this model was adopted to determine the optimal solution[22, 23].

Based on the response surface model of the lever arm, the maximum equivalent force stress, the maximum deformation and the mass of the lever arm were taken as the objective function, and four key dimensions of the lever arm were selected as design variables. In addition, according to the safety factor check method $\sigma_{\max} \leqslant [\sigma] = \sigma_s / n_s$, the yield strength of Q235 was 235MPa, the safety factor was between 1.22.5 and 2.5, and the allowable stress of the material was 94MPa. The mathematical model of multi-objective optimization of lever arm was established as follows:

Objective Function:

$$f(x) = \max f_\sigma(x), \max f_\lambda(x), \min f_n(x), \min f_m(x) \quad (21)$$

Design Variables: $x = [P1, P3, P4, P5]^T$ (22)

Constraints:
$$\begin{cases} \max f_\sigma(x) \le f_\sigma'(x) \\ \max f_\lambda(x) \le f_\lambda'(x) \\ \min f_n(x) \ge f_n'(x) \\ \min f_m(x) \le f_m'(x) \\ \alpha_i \le x_i \le \beta_i \ (i = 1,2,3,4) \end{cases} \quad (23)$$

Where, $\max f_\sigma(x)$ represents the maximum stress, and $\max f_\sigma'(x)$ represents the allowable stress; $\max f_\lambda(x)$ represents the maximum deformation, and $\max f_\lambda'(x)$ represents the maximum allowable deformation; $\min f_n(x)$ represents the minimum safety factor, $\min f_n'(x)$ represents the minimum allowable safety factor; $\min f_m(x)$ represents the minimum mass of the load cross arm, and $\min f_m'(x)$ represents the initial mass of the load cross arm; x_i represents Design Variables, representing 4 key design parameters; α_i represents the lower limit of the change of the design parameters, and β_i represents the upper limit of the change of the design parameters.

B. Multi-objective optimization of genetic algorithm

Multi-objective optimization problems often lead to conflicts among optimization objectives, so it was necessary to compare and weigh the optimal solutions. At present, the NSGA-II algorithm was a recognized multi-objective optimization algorithm, and the multi-objective genetic algorithm was an improved version of the non-dominant ordering genetic algorithm II (NSGA-II), which was based on the basic genetic algorithm, stratifying individuals through non-dominant ordering, and selecting operations according to these stratifications. This strategy significantly improves the algorithm's performance in multi-objective optimization problems by extending the individuals in the Pareto set to the entire set, allowing it to find a set of balanced and satisfactory solutions to meet the needs of multiple competing objectives. The MOGA parameter settings were displayed in Table 5. After nine iterations, the final stability percentage was 1.6929 percent. Fig.12 shows the resulting Pareto optimal dissolution point. The Z axis represents the lever arm mass, the X axis represents the minimum safety factor, the Y axis represents the maximum stress, the three objective functions constitute the spatial coordinate system, and the points in the spatial coordinate system represent various solution sets. The optimal solution set needs to be selected according to the importance of different objective functions.

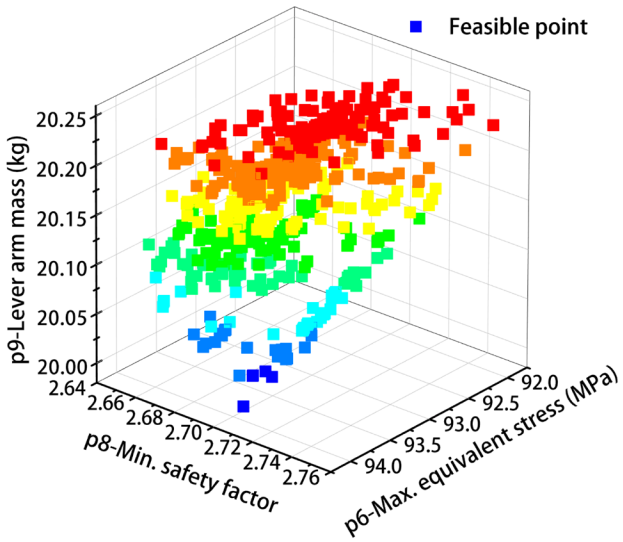

Fig. 12. Pareto optimal solution set

According to the iterative process of each parameter of the lever arm in Fig. 13, the safety factor, maximum equivalent stress and mass in the iterative optimization process did not exceed the set boundary value after 9852 evaluations, and the fluctuation gradually decreased and tended to be stable.

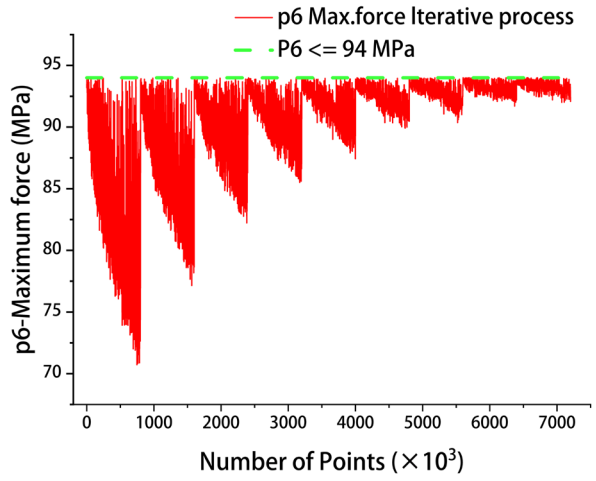

(a) Iterative process of maximum equivalent stress

TABLE V
MOGA PARAMETER SETTINGS

Initial population size	Number of samples per iteration	Max. allowable Pareto percentage/%	Convergence stability percentage /%	Max. number of iterations
4000	800	70	2	20

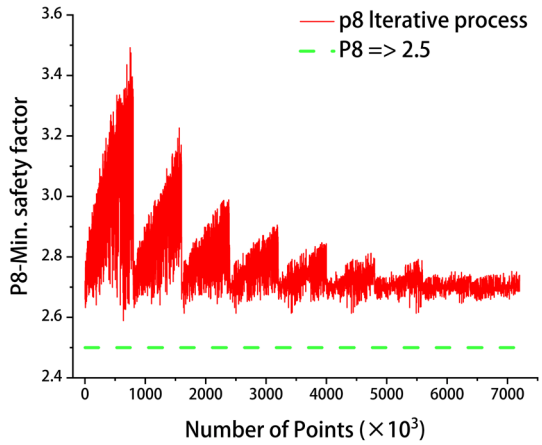

(b) Iterative process of safety factor

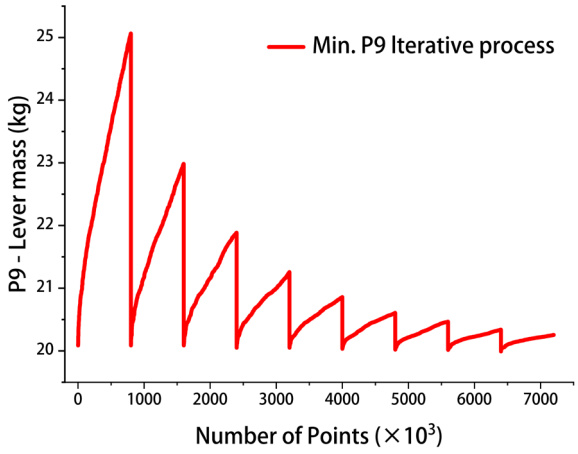

(c) Mass iterative process

Fig. 13. Iterative optimization process of parameters of lever arm

Three groups of optimal candidate points were generated based on the Pareto optimal solution set, as shown in Table 6. Candidate point 2 was chosen as the optimal design point assuming that the lever arm structure meets mechanical property requirements. To address the issue of machining accuracy in the actual machining process, the dimensions of the design parameters were rounded, and the optimized rounding of the design parameters is shown in Table 7.

TABLE VI
CANDIDATE RESULTS

No.	1	2	3
P1/mm	5.09	5.08	5.2
P3/mm	2.44	2.24	3.13
P4/mm	8.19	8.03	8.61
P5/mm	108.54	111.06	103.28
Max. Stress /MPa	93.95	93.84	93.99
Max. Deformation /mm	0.7046	0.6786	0.7598
Min. safety factor	2.7	2.68	2.66
Mass /kg	19.99	20.03	20.06

TABLE VII
COMPARISON OF DESIGN PARAMETERS BEFORE AND AFTER OPTIMIZATION

Target parameters	Before optimization	After optimization	Round /mm
P1	10	5.08	5
P2	80	91.06	91
P3	1	2.24	3
P4	10	8.03	8
P5	100	111.06	111

In order to ensure the reliability of the optimization design results, the size of the optimization design parameters was re-modeled, and the lever arm was analyzed by finite element analysis under the same working conditions, and the optimized results of the target parameters were obtained, as shown in Table 8.

TABLE VIII
COMPARISON OF TARGET PARAMETERS BEFORE AND AFTER OPTIMIZATION

Target parameters	Before optimization	After optimization	Amount of change /%
Max. stress/MPa	123.82	93.843	-24.21
Max. Deformation/mm	0.75597	0.67865	-10.22
Min. safety factor	2.019	2.678	+32.63
Lever arm mass/kg	22.967	20.028	-12.80

According to Table 8, the mass of the optimized lever arm was 12.8% lower than that before optimization, the maximum equivalent stress was reduced by 24.21%, and the deformation was reduced by 10.22%, all of which meet the mechanical performance requirements of the lever arm. The feasibility of the optimal design method has been proved.

V. MODAL ANALYSIS

Modal analysis is a method for studying the dynamic performance of structures, and its applications in the inherent frequency, damping, and mode shapes of structures are relatively mature. Modes can be simply divided into constrained ordinary modes and unconstrained free modes. Ordinary modes have at least one constrained boundary condition, while free modes have no constrained boundary conditions. To study the dynamic performance of the joint, dynamic analysis is required. The general equation of motion for a system with multiple degrees of freedom is:

$$M\ddot{x} + C\dot{x} + Kx = F(t) \tag{24}$$

Where, M represents the generalized mass matrix, C represents the damping matrix, K represents the stiffness matrix, $F(t)$ represents the excitation force vector, $\ddot{x}$, $\dot{x}$, x respectively represent the acceleration, velocity, and displacement response vectors.

For modal analysis, when $F(t)$=0, C can be neglected. The differential equation of kinematics with multiple degrees of freedom is:

$$M\ddot{x} + kx = 0 \tag{25}$$

Its corresponding characteristic equation is:

$$\left(K - \omega^2 M\right)\varphi = 0 \tag{26}$$

Where, ω represents the natural frequency. By solving the above equation, it can be obtained the natural frequencies and mode shapes. The above equation is a polynomial equation in ω, known as the frequency equation, which is a mathematical eigenvalue equation.

Modal analysis of the lever arm can reveal the structure's inherent dynamic characteristics. Modal analysis can be used to determine the natural frequency of each structural component under the modal shape. The natural frequency is only related to the material's elastic modulus, Poisson's ratio, and boundary conditions, with external loads having a minor influence. When performing a modal analysis, constraints must be applied at the connection points between the lever arm and the load weight, the support column rectangular tube, and the load roller. Table 9 shows the modal frequencies of the first six modes, while Fig. 14 depicts their mode shapes.

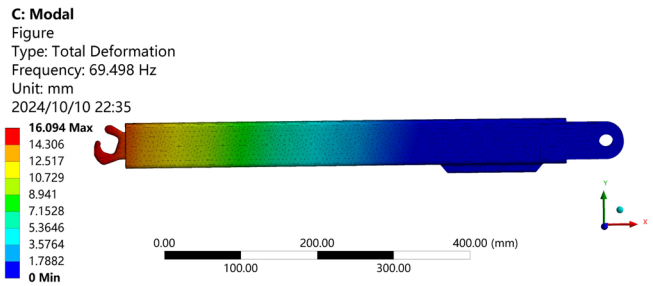

a) First-order mode

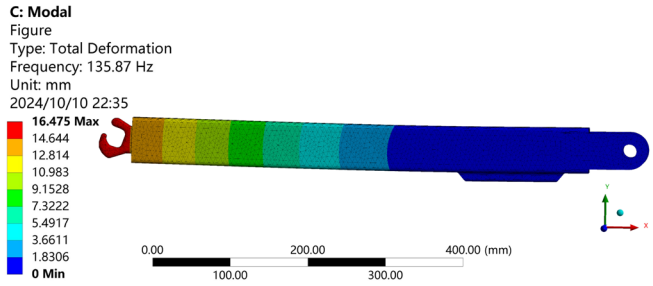

b) Second-order mode

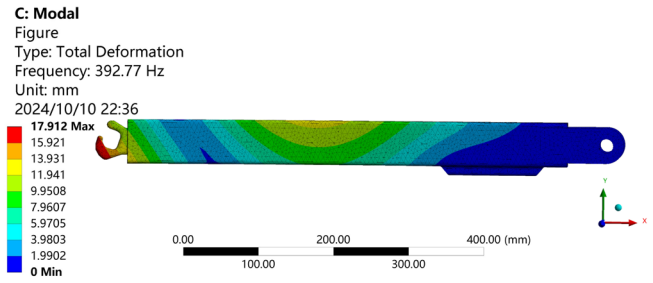

c) Third-order mode

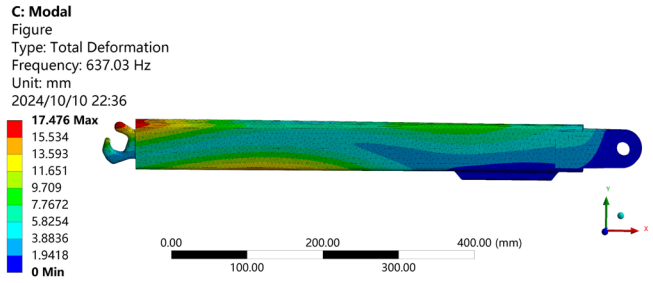

d) Fourth-order mode

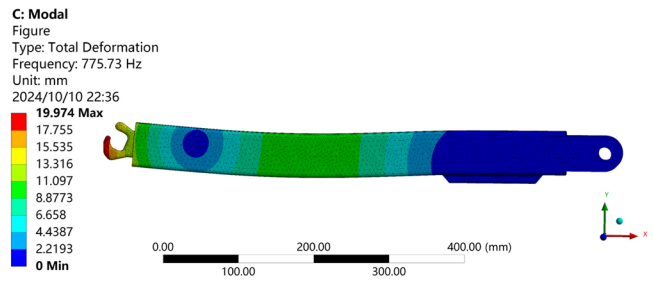

e) Fifth-order mode

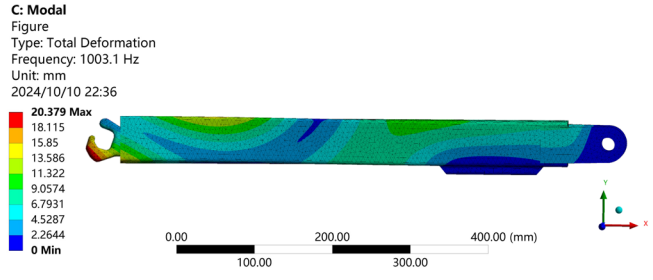

f) Sixth-order mode

Fig. 14. Deformation results of the first six modal shapes

TABLE IX
FIRST SIX NATURAL FREQUENCIES

Mode	1	2	3	4	5	6
Frequency (Hz)	69.49	135.87	392.77	637.03	775.73	1003.1

As shown in Fig. 14, the first six modes of the lever arm are mainly vibration deformations, with the first three modes dominated by frame torsional deformations in the x and y directions, with natural frequencies of 69.49 Hz, 135.87 Hz, and 392.87 Hz, respectively. The fourth to sixth modes are mainly characterized by bending vibrations of the connecting head, with the fourth mode dominated by bending along the x direction, and the fifth and sixth modes dominated by bending along the y direction, with opposite bending directions. The natural frequencies of fourth to sixth modes are 637.03 Hz, 775.73 Hz, and 1003.18 Hz, respectively. The natural frequencies of each order of the lever arm correspond to the vibration trends of the mode shapes, and the first six natural frequencies are much higher than the vibration frequencies generated by the air spring inflation and deflation of the test equipment. Modal analysis shows that the optimized lever arm meets the dynamic structural design requirements.

VI. Installation Test Analysis

As shown in Fig. 15, the optimized lever arm was processed and assembled, and the performance of the lever arm under different working conditions was verified by applying a load on the lever arm hook. The results confirm that the lever arm mounted on the experimental device can meet the test requirements, that the lever arm's design parameters were reasonable, that the mass was effectively reduced, and that the engineering application was good, resulting in the expected design effect, which serves as a reference for the optimal design of similar parts and components.

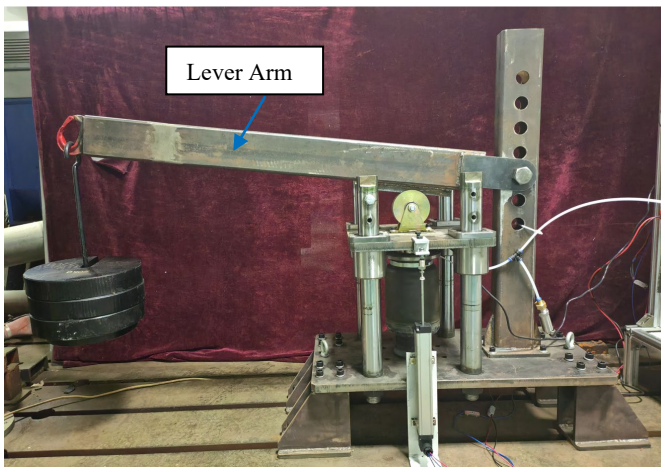

Fig. 15. Application of optimized lever arm working conditions

VII. Conclusion

A response surface optimization design method based on Kriging model and MOGA was proposed for the lightweight design of lever arm of air spring experimental equipment. The specific work and conclusions were as follows:

To begin, use the lever arm of the air spring experimental equipment as a research object, analyze its working principle

and force conditions, parameterize its design structure, and determine the maximum force condition. Next, develop and fit a Kriging response surface model, test its accuracy, and perform sensitivity and response surface analysis on the lever arm. Then seek the optimal Pareto solution set for multi-objective optimization using the NSGA-II algorithm, and select three groups of optimal candidate points. The optimized lever arm has reduced its mass by 12.8%, decreased the maximum equivalent stress by 24.21%, and reduced the maximum deformation by 10.22%. Next, the dynamic characteristics of the lever arm are analyzed in a modal simulation manner, with the natural frequency of the lever arm far exceeding the vibration frequency at which the test equipment operates. Finally, the designed lever arm is processed, assembled, and subjected to engineering tests.

The results show that designing lever arm structures by combining static and dynamic simulation is more reliable and reasonable, while meeting the requirements of lightweight and reliability. This optimization method can provide a solution for the design of similar structures.

REFERENCES

[1] L. Yin, W. Xu, Z. Hu, Y. Zhang, and C. Li,"Performance research and safety verification of compound structure air spring," *Advances in Mechanical Engineering,* vol. 12, no. 12, pp 168-781, 2020.

[2] A. G. Manca, and C. M. Pappalardo, "Topology optimization procedure of aircraft mechanical components based on computer-aided design, multibody dynamics, and finite element analysis.", *Advances in Design, Simulation and Manufacturing III: Proceedings of the 3rd International Conference on Design, Simulation, Manufacturing: The Innovation Exchange*, vol.2, pp 159-168, 2020.

[3] S. A. Ardila-Parra, C. M. Pappalardo, O. A. G. Estrada, and D. Guida,"Finite element based redesign and optimization of aircraft structural components using composite materials," *IAENG International Journal of Applied Mathematics*, vol. 50, no. 4, pp 860-877, 2020.

[4] J. Kudela, and R. Matousek,"Recent advances and applications of surrogate models for finite element method computations: a review," *Soft Computing,* vol. 26, no. 24 , pp 13709-13733, 2022.

[5] S. A. Kouritem, M. I. Abouheaf, N. Nahas, and M. Hassan,"A multi-objective optimization design of industrial robot arms," *Alexandria Engineering Journal,* vol. 61, no. 12, pp 12847-12867, 2022.

[6] J. G. Maradey Lázaro, H. S. Esteban Villegas, and B. J. Blanco Caballero, "Finite Element Analysis (FEA) for Optimization the Design of a Baja SAE Chassis." *ASME International Mechanical Engineering Congress and Exposition,* vol.52033, p. V04AT06A050, 2018.

[7] C. M. Pappalardo, A. G. Manca, and D. Guida,"A Combined Use of the Multibody System Approach and the Finite Element Analysis for the Structural Redesign and the Topology Optimization of the Latching Component of an Aircraft Hatch Door," *IAENG International Journal of Applied Mathematics,* vol. 51, no. 1, pp 175-191, 2021.

[8] L. Shui, F. Chen, A. Garg, X. Peng, N. Bao, and J. Zhang,"Design optimization of battery pack enclosure for electric vehicle," *Structural and Multidisciplinary Optimization,* vol. 58, pp 331-347, 2018.

[9] W. Martinez, C. Cortes, A. Bilal, and J. Kyyra, "Finite element methods for multi-objective optimization of a high step-up interleaved boost converter." *2018 International Power Electronics Conference*, pp. 2193-2198, 2018.

[10] A. Chandrasekhar, and K. Suresh,"TOuNN: Topology optimization using neural networks," *Structural and Multidisciplinary Optimization,* vol. 63, no. 3, pp 1135-1149, 2021.

[11] E. Kurtuluş, A. R. Yıldız, S. M. Sait, and S. Bureerat,"A novel hybrid Harris hawks-simulated annealing algorithm and RBF-based metamodel for design optimization of highway guardrails," *Materials Testing,* vol. 62, no. 3, pp 251-260, 2020.

[12] W. Zhao, and Z. Qiu,"An efficient response surface method and its application to structural reliability and reliability-basedoptimization," *Finite Elements in Analysis and Design,* vol. 67, pp 34-42, 2013.

[13] L. Yang, J. Wang, X. Sun, and M. Xu,"Multi-objective optimization design of spiral demister with punched holes by combining response surface method and genetic algorithm," *Powder Technology,* vol. 355 , pp 106-118, 2019.

[14] C. I. Park,"Multi-objective optimization of the tooth surface in helical gears using design of experiment and the response surface method," *Journal of Mechanical Science and Technology,* vol. 24, pp 823-829, 2010.

[15] C. Wang, Y. Li, W. Zhao, S. Zou, G. Zhou, and Y. Wang,"Structure design and multi-objective optimization of a novel crash box based on biomimetic structure," *International Journal of Mechanical Sciences,* vol. 138, pp 489-501, 2018.

[16] Y.-h. Wang, C. Zhang, Y.-q. Su, L.-y. Shang, and T. Zhang,"Structure optimization of the frame based on response surface method," *International Journal of Structural Integrity,* vol. 11, no. 3, pp 411-425, 2020.

[17] T.-C. Chan, A. Ullah, B. Roy, and S.-L. Chang,"Finite element analysis and structure optimization of a gantry-type high-precision machine tool," *Scientific Reports,* vol. 13, no. 1, pp 13006, 2023.

[18] A. L. Abbas, A. H. Mohammed, and K. S. Abdul-Razzaq,"Finite element analysis and optimization of steel girders with external prestressing," *Civil Engineering Journal,* vol. 4, no. 7, pp 1490-1500, 2018.

[19] J.-H. Zhu, W.-H. Zhang, and L. Xia,"Topology optimization in aircraft and aerospace structures design," *Archives of Computational Methods in Engineering,* vol. 23, pp 595-622, 2016.

[20] S. Koziel, Y. Tesfahunegn, and L. Leifsson,"Variable-fidelity CFD models and co-Kriging for expedited multi-objective aerodynamic design optimization," *Engineering Computations,* vol. 33, no. 8, pp 2320-2338, 2016.

[21] H. Li, J. Gu, M. Wang, D. Zhao, Z. Li, A. Qiao, and B. Zhu,"Multi-objective optimization of coronary stent using Kriging surrogate model," *BioMedical Engineering OnLine,* vol. 15, pp 275-291, 2016.

[22] T. Goel, R. Vaidyanathan, R. T. Haftka, W. Shyy, N. V. Queipo, and K. Tucker,"Response surface approximation of Pareto optimal front in multi-objective optimization," *Computer Methods in Applied Mechanics and Engineering,* vol. 196, no. 4-6, pp 879-893, 2007.

[23] H. Han, B. Li, and W. Shao,"Multi-objective optimization of outward convex corrugated tubes using response surface methodology," *Applied Thermal Engineering,* vol. 70, no. 1, pp 250-262, 2014.